The G protein–coupled receptor GPR31 promotes membrane association of KRAS

Nicole Fehrenbacher,[1] Israel Tojal da Silva,[3] Craig Ramirez,[1] Yong Zhou,[4] Kwang-Jin Cho,[4] Shafi Kuchay,[1,2,5] Jie Shi,[1] Susan Thomas,[1] Michele Pagano,[1,2,5] John F. Hancock,[4] Dafna Bar-Sagi,[1] and Mark R. Philips[1]

[1]Perlmutter Cancer Center and [2]Department of Biochemistry and Molecular Pharmacology, New York University School of Medicine, New York, NY
[3]Laboratory of Molecular Immunology, The Rockefeller University, New York, NY
[4]Department of Integrative Biology and Pharmacology, The University of Texas Medical School at Houston, Houston, TX
[5]Howard Hughes Medical Institute, New York, NY

The product of the *KRAS* oncogene, KRAS4B, promotes tumor growth when associated with the plasma membrane (PM). PM association is mediated, in part, by farnesylation of KRAS4B, but trafficking of nascent KRAS4B to the PM is incompletely understood. We performed a genome-wide screen to identify genes required for KRAS4B membrane association and identified a G protein–coupled receptor, GPR31. GPR31 associated with KRAS4B on cellular membranes in a farnesylation-dependent fashion, and retention of GPR31 on the endoplasmic reticulum inhibited delivery of KRAS4B to the PM. Silencing of GPR31 expression partially mislocalized KRAS4B, slowed the growth of KRAS-dependent tumor cells, and blocked KRAS-stimulated macropinocytosis. Our data suggest that GPR31 acts as a secretory pathway chaperone for KRAS4B.

Introduction

KRAS is the oncogene most frequently mutated in cancer. *KRAS* encodes a small GTPase that regulates signaling pathways for cell growth but functions in this way only when associated with the plasma membrane (PM). Accordingly, much effort has been devoted to understanding how KRAS associates with the PM in the hope of interfering with this process for therapeutic benefit (Cox et al., 2015). KRAS4B, the primary splice variant of the *KRAS* locus, is a peripheral membrane protein that gains affinity for the PM through posttranslational modification of its C-terminal CAAX motif (CVIM sequence) with a farnesyl lipid, followed by endoproteolytic removal of the VIM residues and methyl esterification of the farnesylcysteine. These sequential modifications are catalyzed by farnesyltransferase (FTase), RAS-converting enzyme 1 (RCE1), and isoprenylcysteine carboxylmethyltransferase (ICMT; Wright and Philips, 2006). Modification of the CVIM sequence is necessary but not sufficient for trafficking to the PM; also required is a polybasic sequence in the hypervariable region (HVR) immediately upstream of CVIM (Hancock et al., 1990; Choy et al., 1999). The polybasic sequence allows for an electrostatic interaction with the negatively charged headgroups of the inner leaflet of the PM (Hancock et al., 1990). The interaction can be modulated by phosphorylation of serine 181 within the polybasic region (Bivona et al., 2006).

The characterization of RCE1 (Schmidt et al., 1998) and ICMT (Dai et al., 1998) as polytopic membrane proteins restricted to the ER demonstrated that CAAX processing of RAS and related proteins, begun in the cytosol by FTase, is completed on the cytosolic face of the ER. This has raised the question of how RAS proteins are transferred from the ER to the PM. After CAAX processing, NRAS and HRAS are palmitoylated on the Golgi apparatus and then transferred to the PM via vesicular trafficking (Choy et al., 1999; Apolloni et al., 2000). In contrast, KRAS4B does not visit the Golgi and is not palmitoylated. The mechanism through which nascent KRAS4B traffics from the cytosolic face of the ER to the PM after CAAX processing has not been clearly defined. There is evidence for both rapid, fluid-phase transfer (Silvius et al., 2006) and transfer by vesicular trafficking (Lu et al., 2009; Schmick et al., 2014). Transfer through the cytosol may be facilitated by prenyl-binding proteins such as the δ subunit of phosphodiesterase type 6 (PDE6δ; Chandra et al., 2011; Tsai et al., 2015).

FTase, RCE1, ICMT, and PDE6δ have all served as targets for anticancer drug discovery, but only FTase inhibitors have made it to the clinic, where they failed to show efficacy (Cox et al., 2015). This has stimulated renewed efforts to more fully elucidate the details of RAS trafficking and prompted us to take an unbiased approach to identify previously unrecognized

Correspondence to Mark R. Philips: philim01@nyumc.org;Nicole Fehrenbacher: nfehren01@gmail.com

I.T. da Silva's present address is Laboratory of Computational Biology, A.C. Camargo Cancer Center, São Paulo, Brazil.

Abbreviations used: β_2AR, β_2 adrenergic receptor; FTase, farnesyltransferase; FTI, FTase inhibitor; GGTI, geranylgeranyltransferase inhibitor; GPCR, G protein–coupled receptor; HVR, hypervariable region; ICMT, isoprenylcysteine carboxylmethyltransferase; MP, macropinocytosis; PM, plasma membrane; RCE, RAS-converting enzyme.

The Rockefeller University Press
J. Cell Biol. Vol. 216 No. 8 2329–2338
https://doi.org/10.1083/jcb.201609096

genes involved in targeting KRAS4B to the PM. Our approach led to the discovery of a requirement for and association with GPR31, an orphan G protein–coupled receptor (GPCR). Our data suggest that GPR31 acts as a secretory pathway chaperone to assist in the delivery of KRAS4B from ER to PM.

Results and discussion

Dual-luciferase assay for KRAS4B membrane association

With the goal of performing a screen for previously unappreciated genes required for KRAS4B membrane trafficking, we developed a dual luciferase assay that measures, in a quantitative fashion, the degree of KRAS4B membrane association. We constructed a chimera consisting of a fusion of the DNA-binding domain of Gal4 and the transactivation domain of VP16 fused in turn to the N terminus of KRAS4B (Fig. 1 A). We expected the native PM targeting sequence of KRAS4B to sequester Gal4-VP16 away from the nucleus. We coexpressed this construct with a firefly luciferase reporter driven by a 9xUAS promoter as well as a renilla luciferase driven by a CMV promoter to serve as a control for cell number and transfection efficiency. The resulting expression level of Gal4-VP16-KRAS4B was well below that of endogenous Ras, in part because of proteasomal degradation (Fig. S1 A). Luciferase values were proportional to the amount of Gal4-VP16-KRAS4B plasmid DNA, allowing us to define conditions under which the signal from farnesylation-deficient KRAS4B C185S was 5- to 10-fold higher than WT KRAS4B (Fig. S1 B). Gal4-VP16 fused to the KRAS4B HVR alone (aa 165–188) also required an intact CVIM sequence to mute transcriptional activity but gave higher baseline luciferase values, because this fusion protein was expressed at levels far greater than those of Gal4-VP16-KRAS4B (Figs. 1 B and S1, B and C). The GTP-binding state of the Gal4-VP16-KRAS4B fusion did not affect our assay. We validated the assay by testing KRAS4B C-terminal mutations previously shown to affect membrane binding (Fig. 1 B). As we have reported (Hancock et al., 1990), substituting glutamine for six of the twelve HVR lysines was required to diminish membrane affinity (Fig. 1 B). Although FTase inhibitors (FTIs) alone are ineffective at mislocalizing GFP-KRAS4B because of alternative prenylation (Whyte et al., 1997), a mixture of FTI and a geranylgeranyltransferase inhibitor (GGTI) led to loss of KRAS4B from the PM (Fig. 1 C) and luciferase values similar to those of Gal4-VP16-KRAS4B C185S (Figs. 1 C and S1 C). Silencing *FNTA*, the gene that encodes the common α subunit of FTase and GGTase, also resulted in elevated luciferase readings (Figs. 1 C and S1 D) but did not affect KRAS4B expression (Fig. S3 E). In contrast, silencing neither *RCE1* nor *ICMT* was sufficient to block membrane association of KRAS4B (Fig. S1 D); hence, these genes were not expected to be among screening hits.

Genome-wide siRNA screen for genes that are required for KRAS4B membrane association

We adapted our assay to a 384-well format and performed a genome-wide siRNA screen for genes that, when silenced, gave a firefly/renilla reading above a threshold. siRNA targeting *FNTA* served as the positive control present in multiple wells in all plates (Fig. 1 D). A total of 21,687 genes were screened in duplicate. The Pearson's correlation coefficients for the entire screen were 0.93 for renilla and 0.823 for firefly luciferase. Applying stringent criteria, we identified 100 genes in the library that gave a positive result in the initial screen. Validation assays with alternate siRNAs reduced the number to 26. To those, we applied secondary, independent screens consisting of scoring for mislocalization of GFP-KRAS4B by either inspection or using a previously described (Cho et al., 2012) high-content, image-based assay that measures colocalization by Mander's coefficient of GFP-KRAS4B and cytoplasmic mCherry (Fig. S2; and Table S1). This reduced the number of genes of interest to 13 (Fig. 1 D). Surprisingly, among these were two orphan GPCRs, GPR31 and GPR141. Because GPCRs are among the most amenable to drug treatment of all signaling molecules, we sought to characterize the role of these proteins in KRAS4B membrane association. Ectopically expressed GPR141 proved unstable, so we focused on GPR31. Although silencing *GPR31* was not as effective in reducing the amount of GFP-KRAS4B on the PM as was knockdown of *FNTA*, there was a clear accumulation of GFP-K-Ras4B in the cytoplasm in HeLa (Fig. 1 E), A549 (Fig. S2 A), and U2OS (Fig. S2 B) cells, providing independent validation of a role for GPR31 in KRAS4B membrane association.

KRAS4B interacts with GPR31

Like all GPCRs, GPR31 is predicted to be a seven-membrane–spanning protein that is cotranslationally inserted into the ER and then traffics through the secretory pathway to reach the PM. Consistent with the expected trafficking, live cell imaging revealed GPR31-GFP on the PM and on endomembranes (Fig. 2 A). tdTomato-KRAS4B colocalized with GPR31-GFP. To establish a protein–protein interaction between the colocalized proteins, we expressed HA-tagged GPR31 and GFP-tagged KRAS4B and observed coimmunoprecipitation of the former with the latter (Fig. 2 B). Because expression of properly folded, recombinant GPCRs in the absence of membranes is exceedingly challenging, we could not determine whether the interaction is direct or indirect. HA-GPR31 coimmunoprecipitated with WT KRAS4B but not KRAS4B C185S, demonstrating that farnesylation of KRAS4B is required for the interaction. This was confirmed by treating the cells with FTI plus GGTI, which inhibited the interaction. KRAS4B-CVIL, a construct in which a CAAX motif that directs geranylgeranylation was substituted for the farnesylated CVIM sequence of KRAS4B, also associated with GPR31, demonstrating that either prenyl lipid promotes binding. These results suggest that expression on the same membrane compartment is a prerequisite for the protein–protein interaction. KRAS4B G12V, a constitutively active form, interacted with GPR31 somewhat more efficiently than did the WT protein, suggesting that GTP binding is not required for the interaction but may afford some degree of stabilization.

To establish specificity for GPR31, we tested two other GPCRs. Whereas HA-tagged KRAS4B was coimmunoprecipitated by GPR31-GFP (demonstrating a reciprocal coimmunoprecipitation), neither GFP-tagged β_2 adrenergic receptor (β_2AR) nor a GFP-tagged formyl peptide receptor, FPR-RS2, interacted with the GTPase (Fig. 2 C). To establish specificity for RAS proteins, we tested the other RAS isoforms and a related small GTPase. The alternate splice form of the *KRAS* locus, KRAS4A, interacted with GPR31 as efficiently as did KRAS4B. Both NRAS and HRAS also bound to GPR31, although the interaction with HRAS was less efficient. RAP1b, a small GTPase closely related to RAS, did not bind, demonstrat-

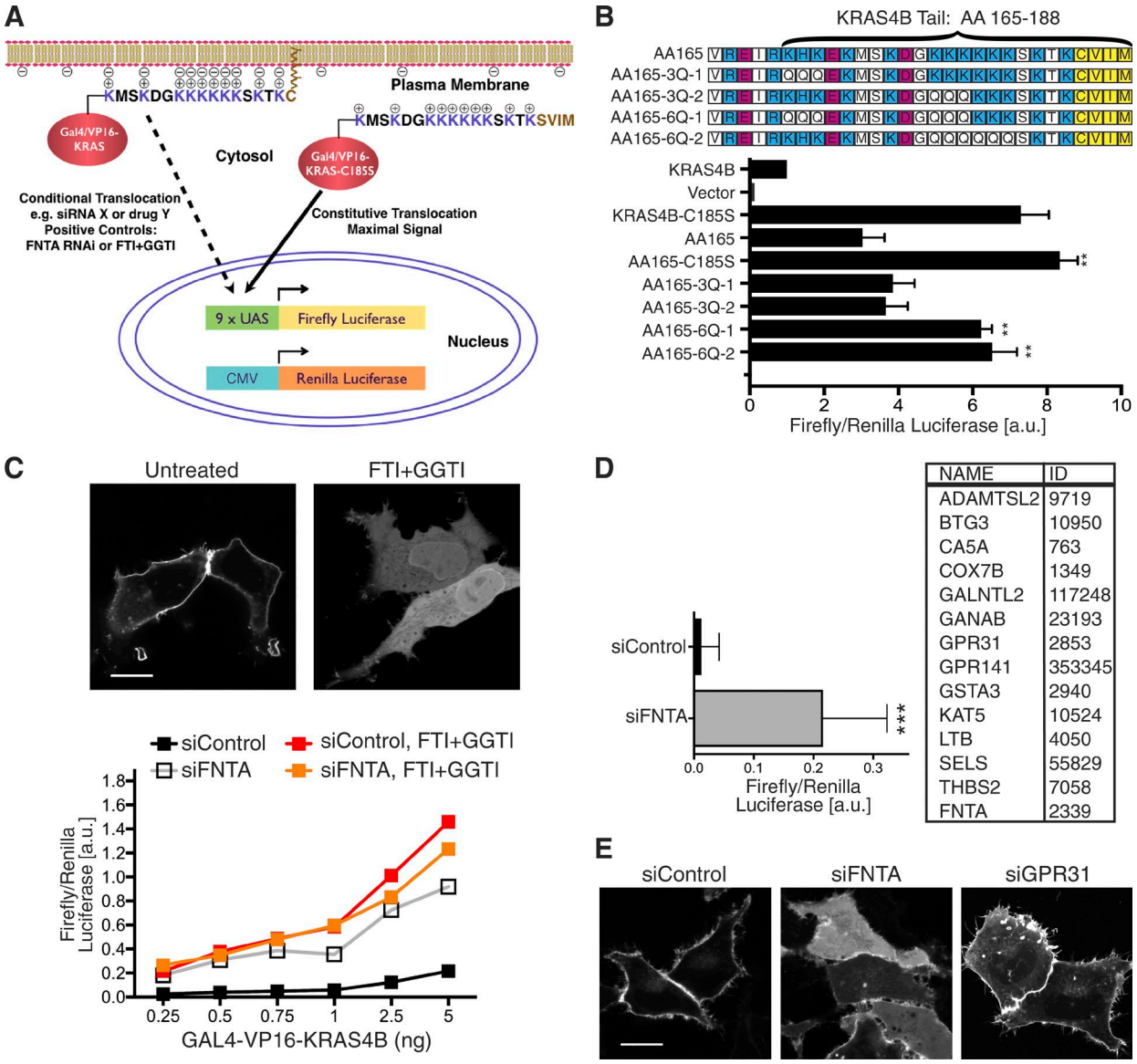

Figure 1. **Genome-wide screen identifies GPR31 as required for KRAS4B membrane association.** (A) KRAS4B membrane association assay. A Gal4-VP16 transcription factor is kept out of the nucleus by fusion with KRAS4B. When expressed in cells that coexpress a 9xUAS firefly luciferase (FL) reporter as well as a CMV-driven renilla luciferase (RL) control, the expression of the reporter is inversely proportional to the affinity for membranes of Gal4-VP16-KRAS4B. Farnesylation-deficient Gal4-VP16-KRAS4B C185S serves as the positive control. (B) Gal4-VP16 was fused to the HVR of KRAS4B (aa 165–188, designated AA165) with or without the indicated substitution of lysines for glutamine and used in the assay described in A. Values plotted are mean ± SD; $n = 3$; **, $P < 0.01$ relative to AA165. (C) Confocal images of live HeLa cells transiently transfected with GFP-KRAS4B and treated with or without FTI + GGTI. HeLa cells transfected with Gal4-VP16-KRAS4B, 9xUAS-FL, and CMV-RL (A) in 384-well format and treated with or without FTI + GGTI or with or without siRNA targeting *FNTA*. Values plotted are representative of two independent experiments. (D) HeLa cells were transfected as in C and subjected to a whole-genome siRNA screen as described in Materials and methods. Positive and negative control values are plotted as mean ± SD of 828 wells distributed among the screening plates. ***, $P < 0.0001$, unpaired *t* test with Welch correction. Table lists 13 genes that scored positive in the screen and were subsequently validated with secondary screens. (E) Confocal images of HeLa cells transfected with GFP-KRAS4B and siRNAs (either nontargeting or targeting *FNTA* or *GPR31*). Bars, 10 µm.

ing specificity for RAS proteins (Fig. 2 D). KRAS interacted with GPR31 when targeted to membranes by either its native C terminus or that of HRAS, but not when targeted with the C terminus of RAP1B (Fig. 2 E). This suggests that the interaction depends both on the G domain of RAS and on proper compartment and membrane microdomain targeting.

GPR31 can retain KRAS4B on endomembrane

The requirement for a GPCR for KRAS4B membrane association and function suggests two alternative models. First is an indirect effect downstream of GPCR signaling. GPR31 has been reported to be a 12-(*S*)-hydroxyeicosatetraenoic acid (12-(*S*)-HETE) receptor that transduces signals to ERK (Guo et al., 2011). Interestingly, GPR31 is up-regulated in prostate cancer (Honn et al., 2016). We have been unable to confirm signaling to ERK, and 12-(*S*)-HETE had no effect on KRAS4B membrane association.

An alternative model is suggested by the protein–protein interaction described. Because GPR31 is an intrinsic membrane protein that transits the secretory pathway, whereas KRAS4B is a peripheral membrane protein with no obvious means of

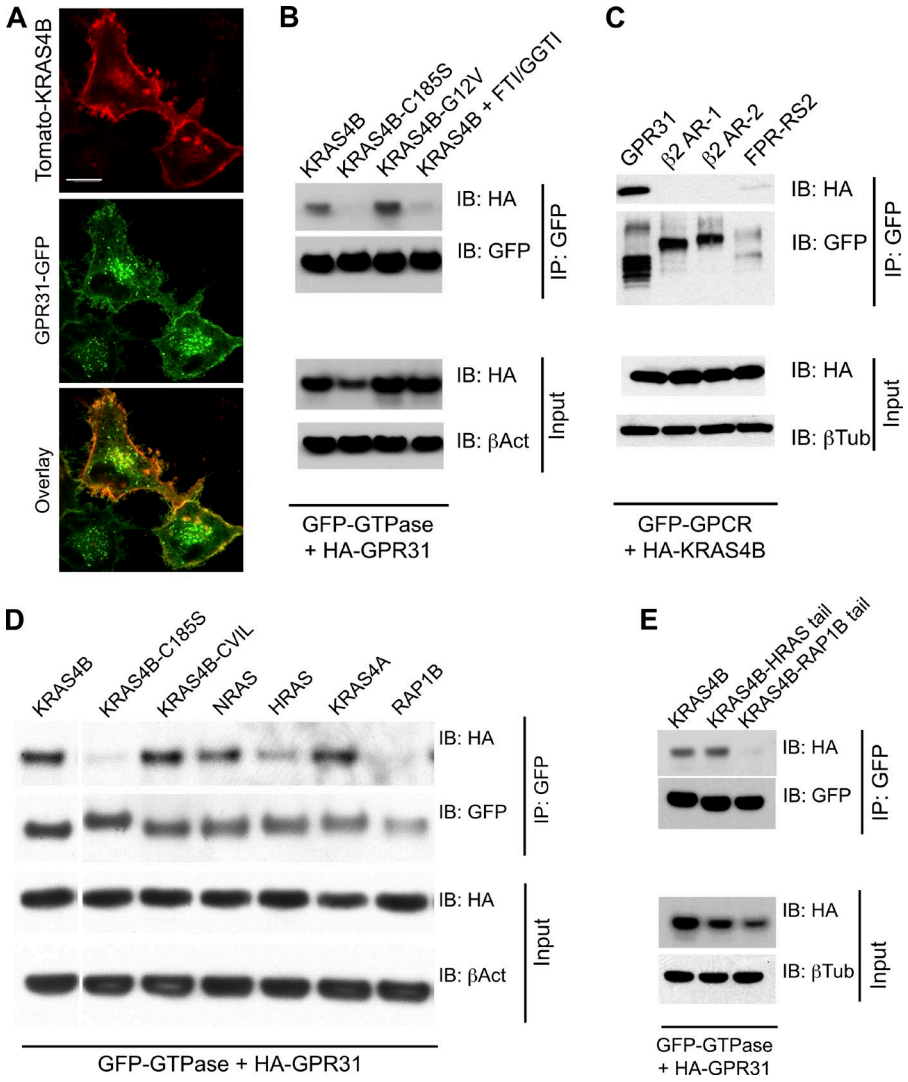

Figure 2. **GPR31 interacts with KRAS4B in a prenylation-dependent manner.** (A) Confocal images of live HeLa cells transiently transfected with GPR31-GFP and tdTomato-KRAS4B. Bar, 10 µm. (B) HEK-293T cells were cotransfected with the indicated GFP-tagged GTPases and HA-tagged GPR31 with or without treatment with FTI + GGTI. GFP-tagged proteins were immunoprecipitated from cell lysates and blotted (IB) for GFP and HA. (C) HEK-293T cells were cotransfected with the indicated GFP-tagged GPCRs and HA-tagged KRAS4B, processed, and analyzed as in B. (D and E) HEK-293T cells were transfected, processed, and analyzed as in B.

active targeting to the PM, we entertained the possibility that GPR31 acts as a secretory pathway chaperone for KRAS4B. One prediction of such a model is that GPR31 retained in the ER might lead to retention of KRAS4B on the same compartment. To test this hypothesis, we appended an ER retention sequence (RSRR; Gassmann et al., 2005) between the GPCR and GFP, coexpressed the modified GPCR with tagged KRAS4B, and observed effects on the localization of the two molecules. As expected, whereas GRP31-GFP decorated both endomembrane and PM, GRP31-RSRR-GFP was restricted to the ER (Fig. 3). Importantly, tdTomato-KRAS4B was observed on the ER when coexpressed with GRP31-RSRR-GFP (Fig. 3 A), supporting the chaperone model. A protein–protein interaction between KRAS4B and GRP31-RSRR-GFP on the ER was confirmed by coimmunoprecipitation (Fig. 3 B). Because silencing GPR31 did not completely inhibit delivery of KRAS4B to the PM (Figs. 1 E and S2) and because relative PM accumulation of GFP-RAS is difficult to quantify by fluorescence, we turned to immunogold EM measurement of GFP-KRAS4B on the basolateral surface of cells, which we have shown to be a highly accurate and reproducible method of measuring PM expression (Prior et al., 2003). We found that silencing GPR31 diminished delivery of KRAS4B to the basolateral membrane of Caco-2 cells by 65% (Fig. 3 C), supporting a model in which GPR31 plays a role in KRAS4B trafficking. Conversely, we observed that overexpression of GPR31 increased delivery of KRAS4B to the basolateral membrane (Fig. 3 D). Importantly, overexpression of ER-restricted GPR31-RSRR had the opposite effect, inhibiting delivery to the PM. These data are consistent with GPR31 playing a role as a trafficking chaperone.

The physical interaction between a GPCR and a RAS family small GTPase has not been previously reported. Nevertheless, such an interaction might be expected given the fact that heterotrimeric G protein α subunits evolved from a primordial small GTPase of the RAS superfamily. Indeed, the recent cocrystal of Gαs complexed with the β_2AR revealed that the GPCR engages the α5 helix of the RAS domain of Gαs (Rasmussen et al., 2011).

GPR31 is required for oncogenic KRAS signaling

We next sought to determine the requirement for GPR31 for KRAS signaling. We were unable to observe a consistent effect on phospho-ERK, MEK, or AKT upon silencing *GPR31*, but neither could we detect consistent changes as a consequence of silencing *KRAS* itself. This is consistent with recent studies of silencing *KRAS* in tumor cells that express mutant *KRAS* (Hayes et al., 2016). We therefore turned to assays of cell growth. We

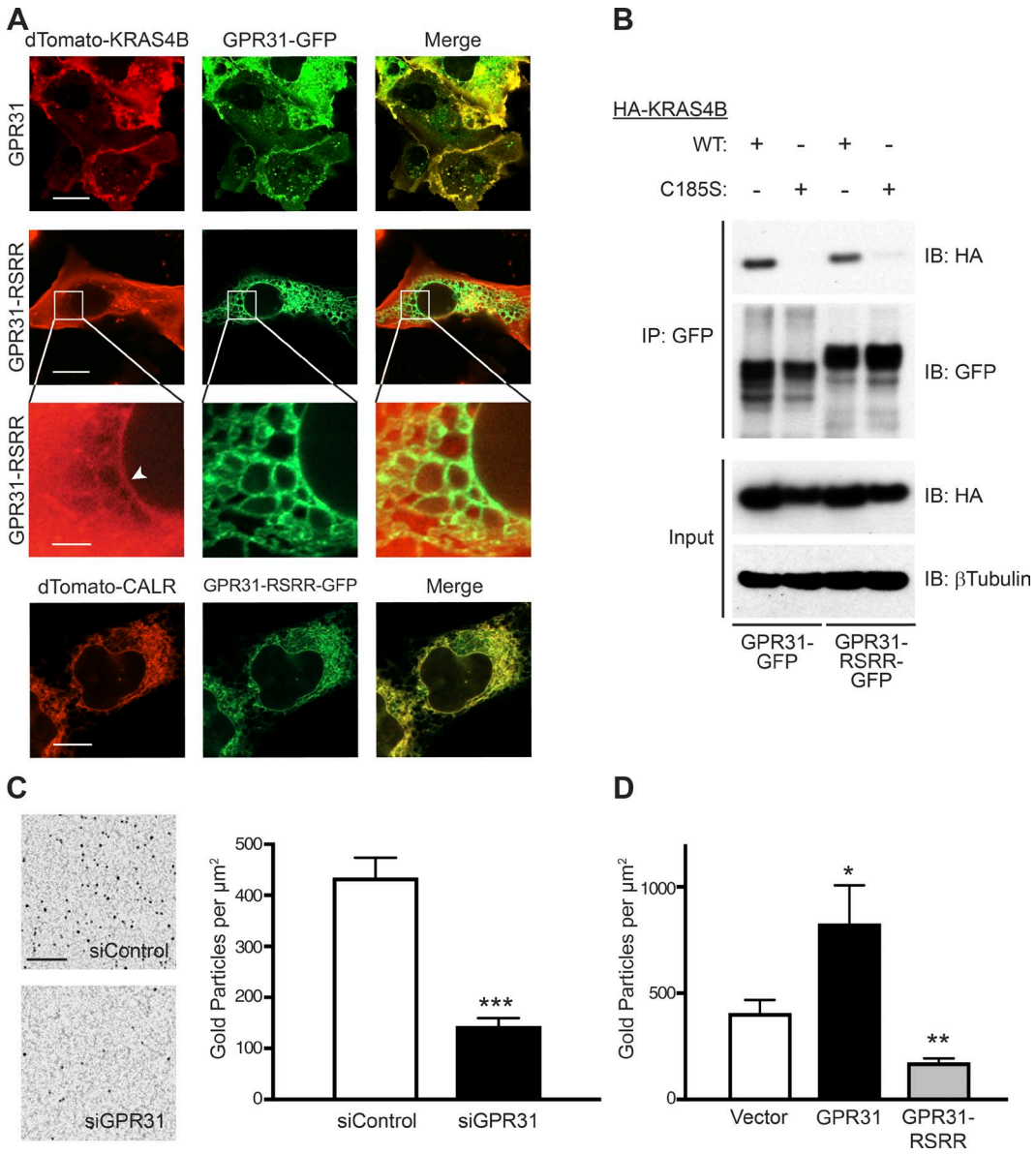

Figure 3. **KRAS4B colocalizes and interacts with GPR31 restricted to the ER, and delivery of KRAS4B to the PM requires GPR31.** (A) COS-1 cells were cotransfected with tdTomato KRAS4B and GPR31-GFP with or without an ER retention signal (RSRR) inserted upstream of GFP and imaged alive as in Fig. 2 A. Enlargement reveals colocalization on the ER. Bars: (main) 10 µm; (enlargements) 2 µm. (B) HEK-293T cells were cotransfected with GFP-tagged GPR31 or GPR31-RSRR and HA-tagged KRAS4B or KRAS4B-C185S. GFP-tagged proteins were immunoprecipitated (IP) from cell lysates and blotted (IB) for GFP and HA. (C) Caco-2 cells were transfected with GFP-KRAS4B and siRNA control or targeting GPR31 before immunogold staining and quantification of GFP-KRAS4B (15 cells analyzed). Bars, 100 nm. (D) BHK cells stably expressing GFP-KRAS4B were transfected with FLAG-tagged GPR31 or GPR31-RSRR and processed as in C (16, 23, and 16 cells analyzed, respectively). Values plotted are mean ± SEM; *, $P < 0.05$; **, $P < 0.01$; ***, $P < 0.001$.

examined the growth of two human tumor cell lines that require KRAS for proliferation, A549 lung adenocarcinoma cells and UM-UC-3 bladder carcinoma cells. Silencing *GPR31* with a number of different siRNAs (Fig. 4) slowed the growth of each of these cells to the same extent as silencing *KRAS* (Fig. 4, A and B; and Fig. S3). HCT116 colon adenocarcinoma cells and MIA-PaCa2 pancreatic adenocarcinoma cells, harboring one or two mutant *KRAS* alleles, respectively, on which they rely for survival (Fleming et al., 2005; Shao et al., 2014), behaved like A549 cells in sensitivity to silencing either *GPR31* or *KRAS* (Fig. 4 C). In contrast, H1437 cells that contain only WT RAS were less sensitive to knockdown of either *GPR31* or *KRAS* (Fig. 4 C). Thus, human cancer cells that require KRAS for survival also require GPR31. We targeted the *GPR31* locus in A549 cells for disruption with CRISPR/Cas9 but were unable to recover any GPR31-null clones, confirming a requirement for GPR31 for survival.

GPR31 is required for KRAS-stimulated macropinocytosis

In addition to stimulating growth and survival, oncogenic KRAS also stimulates macropinocytosis (MP) in tumor cells (Commisso et al., 2013). Using a semiquantitative assay for MP that measures internalized high-molecular-mass dextran, we observed robust uptake in both A549 and UM-UC-3 cells (Fig. 5 A). As expected, silencing *KRAS* dramatically reduced MP in these cells. Strikingly, silencing *GPR31* with any of several siRNAs had the same effect (Fig. 5, A and B). The use of

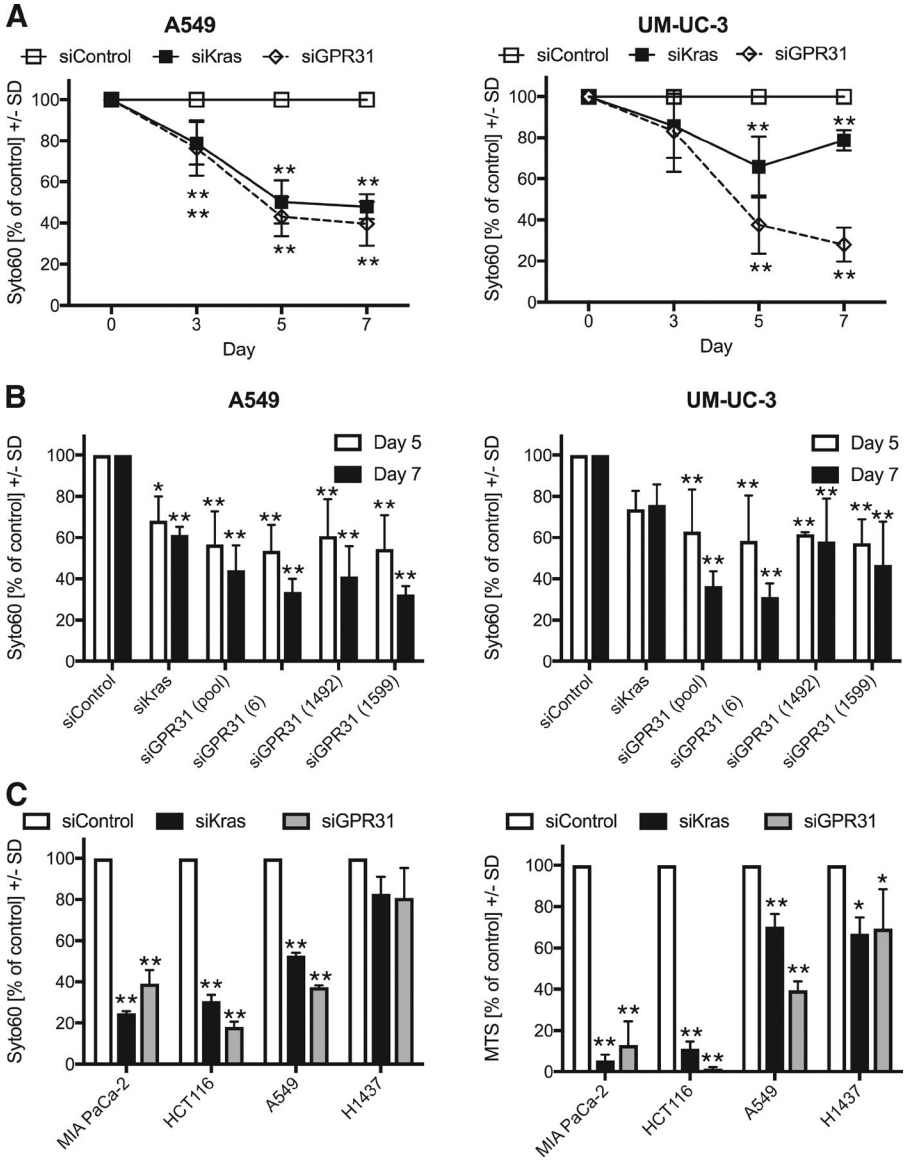

Figure 4. **Depletion of GPR31 slows the growth of KRAS mutant tumor cells.** (A) A549 and UM-UC-3 cells that harbor oncogenic *KRAS* were transfected with control siRNA or siRNA targeting *KRAS* or *GPR31* on day 0. The total number of cells was measured by Syto60 staining on the days indicated. (B) Cells were transfected as in A with the indicated siRNA targeting *GPR31* and harvested on days 5 and 7. (C) Tumor cells with (MIA-PaCa-2, HCT116, A549) or without (H1437) oncogenic *KRAS* were transfected as in A, harvested on day 6, and analyzed for cell number as in A and B or by MTS assay for viability. Values plotted are mean ± SD; n = 6, 4, and 3 for A, B, and C, repectively. *, $P < 0.05$; **, $P < 0.01$.

siRNAs that target the 3′ UTR of the *GPR31* message allowed for expression of exogenous GPR31 without the native UTR. Expression of GPR31 rescued the effect on MP of two siRNAs that target the 3′ UTR, suggesting that the effect of the siRNA is on target (Fig. 5 C).

Oncogenic RAS stimulates MP by engaging TIAM1 (Lambert et al., 2002), which activates RAC1 and thereby enhances PM ruffling. RAS-stimulated MP is not isoform specific because all GTP-bound forms of RAS are capable of stimulating RAC1 through TIAM. To determine whether KRAS4B and GPR31 work in the same pathway with regard to promoting MP, we attempted to rescue the inhibition of MP mediated by silencing GPR31 with overexpression of RAS or RAC1. Ectopic expression of KRAS4B G12V did not overcome the inhibition of MP, either because sufficient expression could not be achieved or because KRAS4B trafficking is sensitive to GPR31 deficiency. In contrast, expression of either HRAS G12V or RAC1 Q61L rescued the effects of silencing GPR31 (Fig. 5 D). This result establishes an epistatic relationship between GPR31 and the RAS/TIAM/RAC1 signaling module with regard to the regulation of MP.

NRAS, HRAS, and KRAS4A are palmitoylated in their HVRs, and this reversible modification works in conjunction with farnesylation to provide an affinity trap on cellular membranes that in turn promotes trafficking via vesicular transport. In contrast, KRAS4B has a relatively low affinity for membranes (Silvius et al., 2006). Although some membrane-to-membrane transport may be effected by fluid phase transfer using cytosolic chaperones such as PDE6δ (Chandra et al., 2011), live cell imaging has also revealed vesicular transport of GFP-KRAS4B (Lu et al., 2009). The notion of a KRAS4B transport chaperone that is itself a transmembrane protein that transits the secretory pathway from ER to cell surface is an attractive one. All seven-transmembrane–spanning proteins do not necessarily function by signaling to heterotrimeric G proteins. For example, there is a large class of "GPCRs" that serve as adhesion molecules (Yona et al., 2008) and smoothened functions without G proteins (Ayers and Thérond, 2010). Our data suggest yet another function of a specific GPCR, that of assisting KRAS4B to navigate the secretory pathway to the PM where it signals. The requirement for GPR31 for growth of *KRAS*-transformed cells suggests that the protein–protein interaction reported here

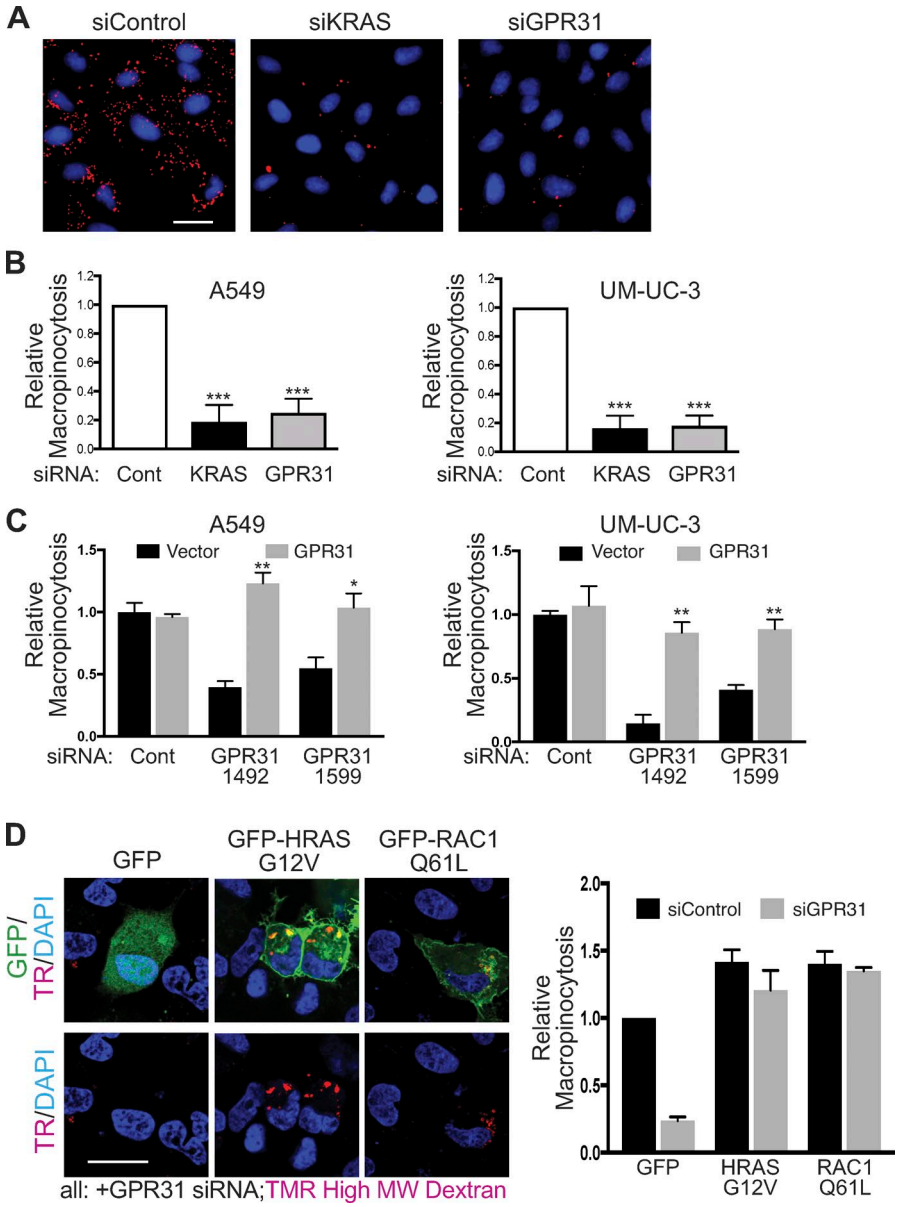

Figure 5. **GPR31 is required for *KRAS*-dependent macropinocytosis.** (A) A549 cells were transfected with control siRNA or siRNA targeting KRAS or GPR31 and analyzed for macropinocytosis as described in Materials and methods. Representative micrographs are shown with HMW dextran in red and nuclei in blue. (B) Quantification of data shown in A for both A549 and UM-UC-3 cells. (C) Macropinocytosis quantified as in B in cells treated with the indicated siRNA targeting GPR31 with or without forced expression of GPR31 as indicated. (D) A549 cells treated with or without siRNA targeting GPR31 were transfected with GFP alone, GFP-HRAS G12V, or GFP-RAC1 Q61L. GFP-positive cells were analyzed for macropinocytosis. Representative micrographs of cells treated with siGPR31 are shown with HMW dextran in red, nuclei in blue, and GFP in green. Bar graph shows quantification of macropinocytosis in cells positive for GFP. Values plotted are mean ± SD; $n = 3$; **, $P < 0.01$; ***, $P < 0.0001$. Bars, 10 µm.

is functionally important and raises the possibility of a new target for anti-RAS therapy.

Materials and methods

Luciferase-based assay measuring KRAS4B membrane association

HeLa cells were plated in 96-well plates the day before transfection. The GAL4 DNA binding domain (aa 1–147) linked to a VP16 full-length activation domain (aa 413–490; Ogura et al., 2009) was subcloned into pCDNA3.1(+) (Thermo Fisher Scientific). The coding sequence of full-length KRAS4B or the KRAS4B hypervariable region (aa 165–188) was cloned in-frame 3′ of the Gal4-VP16 sequence. Various mutants were created using standard cloning procedures. HeLa cells were cotransfected using SuperFect (QIAGEN) with the indicated GAL4-VP16 chimeras along with UAS-firefly luciferase (pGL4.35, luc2P/9xGAL4UAS/Hygro, #137A; Promega) and CMV-renilla luciferase (gift from R. Dasgupta, Genome Institute of Singapore, Singapore). Where indicated, a combination of FTI L-744,832 and GGTI-2418 was added 2–4 h after transfection. Cells were harvested, lysed, and assayed for firefly and renilla luciferase activities according to the protocol for the Dual-Glo Luciferase Assay System (Promega).

Human whole-genome siRNA screen

A whole-genome siRNA screen was performed in HeLa cells using a prealiquoted Silencer siRNA library (Ambion) at 30 nM final concentration. A total of 21,687 genes were represented in the library and were arrayed into sixty-nine 384-well plates in duplicate. Gene silencing was induced for 72 h via reverse transfection using Dharmafect 1 (GE Healthcare). Thereafter, the cells were transfected with the reporter constructs (GAL4-VP16-KRAS4B, UAS-firefly luciferase, and CMV-renilla luciferase), and 24 h later the luciferase activities (firefly and renilla) were measured according to the manufacturer's instructions (Promega). The renilla luciferase served as internal control for transfection efficiency and cell viability. The Pearson's correlation coefficients of the renilla raw values were 0.885 for the negative nontargeting control siRNA and 0.893 for the positive control siRNA targeting *FNTA*. The Pearson's correlation coefficients for the entire screen were 0.93 for renilla luciferase and 0.823 for firefly luciferase raw values. Normalization of the firefly luciferase values to renilla luciferase values

were used for further evaluation. The *Kif11* siRNA that targets a gene essential for cell survival served as control for knockdown efficiency. As expected, wells that received *Kif11* siRNA had very low renilla luciferase values, leading to elevated firefly/renilla ratios in the absence of stimulated firefly luciferase activity. To avoid scoring false positives because of the down-regulation of essential genes, wells with renilla values lower than 1,000 were eliminated from further analysis. Mean firefly/renilla luciferase values were calculated for each plate for both the entire set of wells and those wells containing negative control siRNAs. *z*-Scores for each well were calculated as the difference between the plate mean and an individual well, divided by the SD of each plate. The values for each gene were analyzed by three methods. In method 1, the value for each well was divided by the plate mean. In method 2, the value for each well was divided by the negative control mean. In method 3, the *z*-score for each well was divided by the mean *z*-score of the negative control wells for the entire screen. Genes were marked as potentially positive for each method if the normalized values reached values 5-, 7-, or 10-fold that of the denominator. Hits were selected as those genes that reached a 7- or 10-fold threshold in at least two of the three methods of analysis or reached the fivefold threshold in all three methods. 100 of the 21,687 genes screened met these criteria. These genes were then evaluated with a validation screen with three individual siRNAs. 26 genes passed the validation screen with firefly/luciferase values ≥2-fold higher than nontargeting siRNAs induced by at least two of the three siRNAs tested and in at least two of three replica plates. The 26 genes identified were further validated with an independent secondary screen involving silencing each gene with GE Healthcare SmartPool ON-TARGET plus siRNA in HeLa cells expressing GFP-KRAS4B and scoring for mislocalization of the fluorescent protein from the plasma membrane to the cytoplasm. Mislocalization of GFP-KRAS4B was also performed in a quantitative manner using Mander's coefficient (see Determination of Mander's coefficient).

CRISPR/Cas9-gene targeting

The sequence to be targeted in the *GPR31* locus was generated by annealing the following oligos: top, 5′-CACCGCGCCTTCTACCTG AGCCTCC-3′, and bottom, 5′- AAACGGAGGCTCAGGTAGAAG GCGC-3′, and cloned into pSpCas9(BB)-2A-GFP (PX458) to direct expression of a sgRNA along with Cas9, as described (Ran et al., 2013). To insert a premature stop codon into this locus, a single-stranded DNA oligo encoding a repair template for homologous recombination was designed with the following sequence: 5′-GTCTACCTGCTCAAC CTGGCCCTGGCTGACCTGCTGTTGGCTGCGTGCCTGCCTTTC CTGGCCGCCTTCTACCTGAGCCTCCAAGCTTGGCATCTG**TG A**CGTGTGGGCTGCTGGGCCCTGCACTTCCTGCTGGACCTC AGCCGCAGCGTGGGGATGGCCTTCCTGGCCGCCGTGGCT TTGGACCGGTACCTCCGTGTGGT-3′ (inserted stop codon in bold).

A549 cells were cotransfected with pSpCas9(BB)-2A-GFP-GPR31 and the repair template using Lipofectamine 3000 (Invitrogen). Cells were sorted for GFP expression and seeded as single-cell clones. Clones were screened for genome editing by PCR with the following primer pairs: WT forward, 5′-CCAGGCTTGGCATCT GGGC-3′, and reverse, 5′-AGTGCTTCCTGCCAGATGAT-3′; mutant forward, 5′-CCAAGCTTGGCATCTGTGA-3′, and reverse, 5′-AGTGCTTCCTGCCAGATGAT-3′.

Determination of Mander's coefficient

Human lung adenocarcinoma A549 cells (3.2×10^4 cells) were mixed with 320 nM siRNA and transfection reagent (Dharmafect I) and plated in triplicate in a 96-well plate (Matrical). After 48 h, plated cells were retransfected with 320 nM siRNA. After a further 72 h, cells were infected with lentivirus coexpressing mGFP-tagged K-RasG12V and mCherry-CAAX, an endomembrane marker (Choy et al., 1999). Incubation was continued for 24 h to allow expression of the fluorescently labeled proteins. Cells were then fixed with 4% PFA and imaged using a confocal microscope. PM mislocalization of mGFP-KRASG12V was quantified using Mander's coefficient, to measure the fraction of mCherry-CAAX colocalizing with mGFP-KRASG12V as previously described (Cho et al., 2012).

Immunoprecipitation and immunoblotting

HEK-293T cells were plated on 10-cm dishes and transfected with Lipofectamine 3000 (Invitrogen) with plasmids directing expression of epitope-tagged GPR31 or RAS proteins. 20 h later, the cells were lysed (50 mM Tris, pH 8.0, 150 mM NaCl, 10% glycerol, 1 mM EDTA, 50 mM NaF, and 0.1% NP-40), and the lysates were clarified by centrifugation. Immunoprecipitation and Western blotting were performed as previously described (Kuchay et al., 2013) with GFP-conjugated agarose beads (D153-8; MBL International). Direct immunoblots (without prior immunoprecipitation) were performed with the primary antibodies (see Antibodies, plasmids, and chemicals) and detected with IRDye secondary antibodies (LI-COR Biosciences) that were visualized and quantified using an Odyssey scanner (LI-COR Biosciences).

Immunogold EM

Immunogold-labeling of basolateral PM was performed as described (Prior et al., 2003). Caco-2 cells transiently expressing GFP-KRASG12V (lentiviral transduction) or BHK cells stably expressing GFP-K-RASG12V were transfected with siRNA (Caco-2) or FLAG-tagged WT GPR31 or GPR31-RSRR (BHK). Intact apical PM sheets of the cells were attached to copper EM grids, fixed with 4% PFA and 0.1% glutaraldehyde, immunolabeled with 4.5 nm gold nanoparticles coupled to anti-GFP antibody, and embedded in uranyl acetate. PM sheets were imaged using transmission EM at 100,000× magnification. Numbers of gold particles were counted within selected 1-μm^2 PM areas. At least 15 individual PM sheets were imaged and analyzed for each condition.

Macropinosome visualization and quantification

A549 and UM-UC-3 cells were plated onto glass coverslips, transfected the next day with siRNAs using Dharmafect 1 or RNAiMAX (Invitrogen), and examined after 72 h. Where indicated, cells were transfected again after 48 h using Lipofectamine 3000 (Invitrogen) with pEGFP empty vector or pEGFP-N1-GPR31. Macropinocytosis was quantified as previously described (Commisso et al., 2013, 2014). In brief, cells were serum-starved for 3 h. Macropinosomes were marked using a high-molecular-mass TMR-dextran uptake assay wherein TMR-dextran (Fina Biosolutions) was added to serum-free medium at a final concentration of 1 mg/ml for 30 min at 37°C. At the end of the incubation period, cells were rinsed five times in cold PBS and immediately fixed in 3.7% formaldehyde. Cells were DAPI-treated to stain nuclei, and coverslips were mounted onto slides using Dako Mounting Media. Images were captured using an Axiovert 200 inverted fluorescent microscope (ZEISS) and analyzed using the "analyze particles" feature in ImageJ (National Institutes of Health). The total particle area per cell was determined from at least five fields that were randomly selected from different regions across the entirety of each sample.

Antibodies, plasmids, and chemicals

The following antibodies were purchased from commercial sources: HA antibody (Covance), GFP antibody (D5.1; Cell Signaling Technology), β-actin (AC-74; Sigma-Aldrich), VP16 (ab4808-100; Abcam), RAS (Ab-3, OP40; EMD Millipore), ERK1 (sc-94, K-23; Santa Cruz Biotechnology, Inc.), and β-tubulin (E7-s; Developmental Studies Hybridoma Bank). GFP-agarose beads (D153-8) were from MBL Inter-

national. pCXN2-HA-human GPR31 was obtained from J. Miyazaki (RIKEN Center for Developmental Biology, Kobe, Japan; Niwa et al., 1991). Human GPR31 was inserted into pCGN-HA vector and pEGFP-N1 by standard PCR cloning. Human β2AR was inserted into pEGFP-N1 (β_2AR-1) and was also obtained in S65TGFP vector (β_2AR-2) from L. Barak (Duke University, Durham, NC). The mouse formyl peptide receptor FPR-rs2 was received in pEGFP-N1 vector from P. Murphy (National Institute of Allergy and Infectious Diseases, Bethesda, MD). The peptide sequence from rat GABA receptor 1b, which contains the ER localization signal RSRR (LLEKENRELEKI IAEKEERVSELRHQLQSRQQLRSRR), was linked to the 3′ end of Flag-GPR31 (human) and cloned into pEGFP-N1. KRAS4B was cloned from pEGFP-C3-KRAS4B into ptdTomato-C1. FTI L-744,832 was purchased from Enzo Life Sciences, and GGTI-2418 was provided by S. Sebti (Moffitt Cancer Center, Tampa, FL).

Live cell imaging

Cells were plated in 35-mm dishes with a 14-mm round cutout covered by a 1.5 glass coverslip (MatTek Corporation) in DMEM medium supplemented with 10% FBS overnight before transfection with siRNA for 48 h and thereafter with GFP-KRAS4B for an additional 20 h. Transfection with siRNA was performed with Dharmafect 1 or RNAiMax (Invitrogen), and plasmid transfection with Lipofectamine 2000 or 3000 reagents. Medium change occurred 1 h after plasmid transfection with fresh medium. Right before imaging cells, medium was changed to OptiMEM. Live cell imaging was performed with an inverted LSM 510 META or LSM 800 microscope (ZEISS) equipped with ZEN image processing software, using a Plan-Apochromat 63× NA 1.4 oil objective under conditions of 37°C and 5% CO_2.

Syto60 staining and MTS assay

A549, UM-UC-3, MIA-PaCa-2, HCT116, and H1437 cells were transfected with siRNA on day 0 via reverse transfection using Dharmafect 1 or RNAiMAX at a final concentration of 30 nM and plated in regular 96-well plates for MTS assay or black 96-well plates with clear bottoms for Syto60 staining (Costar 3603). At indicated times, cells were harvested for MTS assay according to the manufacturer's instructions (Promega G3580). Absorbance was measured at 490 nm. For Syto60 staining, cells were permeabilized with 0.1% Triton X-100 in PBS, and nuclei were stained with a 1:5,000 dilution of Syto60 reagent (S11342; Thermo Fisher Scientific) before analyzing wells for red fluorescence with an Odyssey scanner (LI-COR Biosciences).

Gene silencing with siRNA

HeLa, A549, UM-UC-3, MIA-PaCa-2, HCT116, and H1437 cells were transfected with siRNA with either Dharmafect1 or RNAiMAX at 30 nM final concentration. Dharmacon smartpool ON-TARGETplus siRNAs (GE Healthcare) were used for the following genes: *GPR31* (L-005564-00), *FNTA* (L-008807-00), *KRAS* (L-005069-00), and control nontargeting (D-001810-10-20). The single siRNA targeting *GPR31* from the smartpool, *GPR31*_6 (J-005564-06), was also used. Additional single siRNAs targeting the 3′ UTR region of *GPR31* were of Stealth RNAi configuration (Thermo Fisher Scientific): *GPR31*_1492 (U65402_1492; Thermo Fisher Scientific) and *GPR31*_1599 (U65402_1599; Thermo Fisher Scientific).

Statistical analysis

For Syto60 staining and MTS assays, statistical analysis was performed relative to siControl using ANOVA with Dunnett's posttest. For macropinocytosis and immunogold EM assays, statistical analysis was performed relative to siControl or vector using unpaired Student's *t* test.

Online supplemental material

Fig. S1 shows the verification of the dual luciferase assay for measuring KRAS4B membrane association. Fig. S2 shows the siRNA-induced mislocalization of GFP-KRAS4B. Fig. S3 confirms that siRNA knockdown reduces GPR31 protein levels. Table S1 shows quantification of GFP-KRAS4B G12V siRNA-induced mislocalization from the PM.

Acknowledgments

We thank Lawrence Barak, Yusuke Kamachi, Jun-ichi Miyazaki, Philip Murphy, Toshiaki Okuno, Said Sebti, and Senji Shirasawa for reagents. We thank Ramanuj Dasgupta and Chi Yun for assistance with the siRNA screen.

This work was supported by the National Institutes of Health (GM55279, GM057587, CA116034, CA163489, CA076584, T32HL7151, and P30CA16087), National Institutes of Health/National Cancer Institute (CA210263), NYSTEM (C026719 and N11G-255), Shifrin-Meyer Breast Cancer Discover Fund, Deutsche Akademie der Naturforscher Leopoldina (BMBF-LPD 9901/8-180), and the Revson Foundation.

The authors declare no competing financial interests.

Author contributions: N. Fehrenbacher and M.R. Philips designed the study, interpreted the results, and wrote the manuscript. N. Fehrenbacher performed and interpreted the genome-wide screen and performed or directed all the follow-up experiments. I.T. da Silva assisted N. Fehrenbacher with the bioinformatic analysis of the genome-wide siRNA screen. N. Fehrenbacher and C. Ramirez performed the macropinocytosis assays. Y. Zhou performed the immunogold EM analysis. K.-J. Cho performed the Mander's quantification of GFP-KRAS4B mislocalization for the validation assay. S. Kuchay assisted with coimmunoprecipitations. J. Shi and S. Thomas provided technical assistance. M. Pagano, J.F. Hancock, and D. Bar-Sagi provided expert consultation.

Submitted: 21 September 2016
Revised: 5 April 2017
Accepted: 12 May 2017

References

Apolloni, A., I.A. Prior, M. Lindsay, R.G. Parton, and J.F. Hancock. 2000. H-ras but not K-ras traffics to the plasma membrane through the exocytic pathway. *Mol. Cell. Biol.* 20:2475–2487. http://dx.doi.org/10.1128/MCB.20.7.2475-2487.2000

Ayers, K.L., and P.P. Thérond. 2010. Evaluating Smoothened as a G-protein-coupled receptor for Hedgehog signalling. *Trends Cell Biol.* 20:287–298. http://dx.doi.org/10.1016/j.tcb.2010.02.002

Bivona, T.G., S.E. Quatela, B.O. Bodemann, I.M. Ahearn, M.J. Soskis, A. Mor, J. Miura, H.H. Wiener, L. Wright, S.G. Saba, et al. 2006. PKC regulates a farnesyl-electrostatic switch on K-Ras that promotes its association with Bcl-XL on mitochondria and induces apoptosis. *Mol. Cell.* 21:481–493. http://dx.doi.org/10.1016/j.molcel.2006.01.012

Chandra, A., H.E. Grecco, V. Pisupati, D. Perera, L. Cassidy, F. Skoulidis, S.A. Ismail, C. Hedberg, M. Hanzal-Bayer, A.R. Venkitaraman, et al. 2011. The GDI-like solubilizing factor PDEδ sustains the spatial organization and signalling of Ras family proteins. *Nat. Cell Biol.* 14:148–158. http://dx.doi.org/10.1038/ncb2394

Cho, K.J., J.H. Park, A.M. Piggott, A.A. Salim, A.A. Gorfe, R.G. Parton, R.J. Capon, E. Lacey, and J.F. Hancock. 2012. Staurosporines disrupt phosphatidylserine trafficking and mislocalize Ras proteins. *J. Biol. Chem.* 287:43573–43584. http://dx.doi.org/10.1074/jbc.M112.424457

Choy, E., V.K. Chiu, J. Silletti, M. Feoktistov, T. Morimoto, D. Michaelson, I.E. Ivanov, and M.R. Philips. 1999. Endomembrane trafficking of ras: The CAAX motif targets proteins to the ER and Golgi. *Cell.* 98:69–80. http://dx.doi.org/10.1016/S0092-8674(00)80607-8

Commisso, C., S.M. Davidson, R.G. Soydaner-Azeloglu, S.J. Parker, J.J. Kamphorst, S. Hackett, E. Grabocka, M. Nofal, J.A. Drebin, C.B. Thompson, et al. 2013. Macropinocytosis of protein is an amino

acid supply route in Ras-transformed cells. *Nature.* 497:633–637. http://dx.doi.org/10.1038/nature12138

Commisso, C., R.J. Flinn, and D. Bar-Sagi. 2014. Determining the macropinocytic index of cells through a quantitative image-based assay. *Nat. Protoc.* 9:182–192. http://dx.doi.org/10.1038/nprot.2014.004

Cox, A.D., C.J. Der, and M.R. Philips. 2015. Targeting RAS membrane association: Back to the future for anti-RAS drug discovery? *Clin. Cancer Res.* 21:1819–1827. http://dx.doi.org/10.1158/1078-0432.CCR-14-3214

Dai, Q., E. Choy, V. Chiu, J. Romano, S.R. Slivka, S.A. Steitz, S. Michaelis, and M.R. Philips. 1998. Mammalian prenylcysteine carboxyl methyltransferase is in the endoplasmic reticulum. *J. Biol. Chem.* 273:15030–15034. http://dx.doi.org/10.1074/jbc.273.24.15030

Fleming, J.B., G.L. Shen, S.E. Holloway, M. Davis, and R.A. Brekken. 2005. Molecular consequences of silencing mutant K-ras in pancreatic cancer cells: Justification for K-ras-directed therapy. *Mol. Cancer Res.* 3:413–423. http://dx.doi.org/10.1158/1541-7786.MCR-04-0206

Gassmann, M., C. Haller, Y. Stoll, S. Abdel Aziz, B. Biermann, J. Mosbacher, K. Kaupmann, and B. Bettler. 2005. The RXR-type endoplasmic reticulum-retention/retrieval signal of GABAB1 requires distant spacing from the membrane to function. *Mol. Pharmacol.* 68:137–144.

Guo, Y., W. Zhang, C. Giroux, Y. Cai, P. Ekambaram, A.K. Dilly, A. Hsu, S. Zhou, K.R. Maddipati, J. Liu, et al. 2011. Identification of the orphan G protein-coupled receptor GPR31 as a receptor for 12-(S)-hydroxyeicosatetraenoic acid. *J. Biol. Chem.* 286:33832–33840. http://dx.doi.org/10.1074/jbc.M110.216564

Hancock, J.F., H. Paterson, and C.J. Marshall. 1990. A polybasic domain or palmitoylation is required in addition to the CAAX motif to localize p21ras to the plasma membrane. *Cell.* 63:133–139. http://dx.doi.org/10.1016/0092-8674(90)90294-O

Hayes, T.K., N.F. Neel, C. Hu, P. Gautam, M. Chenard, B. Long, M. Aziz, M. Kassner, K.L. Bryant, M. Pierobon, et al. 2016. Long-term ERK inhibition in KRAS-mutant pancreatic cancer is associated with MYC degradation and senescence-like growth suppression. *Cancer Cell.* 29:75–89. http://dx.doi.org/10.1016/j.ccell.2015.11.011

Honn, K.V., Y. Guo, Y. Cai, M.J. Lee, G. Dyson, W. Zhang, and S.C. Tucker. 2016. 12-HETER1/GPR31, a high-affinity 12(S)-hydroxyeicosatetraenoic acid receptor, is significantly up-regulated in prostate cancer and plays a critical role in prostate cancer progression. *FASEB J.* 30:2360–2369. http://dx.doi.org/10.1096/fj.201500076

Kuchay, S., S. Duan, E. Schenkein, A. Peschiaroli, A. Saraf, L. Florens, M.P. Washburn, and M. Pagano. 2013. FBXL2- and PTPL1-mediated degradation of p110-free p85β regulatory subunit controls the PI(3)K signalling cascade. *Nat. Cell Biol.* 15:472–480. http://dx.doi.org/10.1038/ncb2731

Lambert, J.M., Q.T. Lambert, G.W. Reuther, A. Malliri, D.P. Siderovski, J. Sondek, J.G. Collard, and C.J. Der. 2002. Tiam1 mediates Ras activation of Rac by a PI(3)K-independent mechanism. *Nat. Cell Biol.* 4:621–625.

Lu, A., F. Tebar, B. Alvarez-Moya, C. López-Alcalá, M. Calvo, C. Enrich, N. Agell, T. Nakamura, M. Matsuda, and O. Bachs. 2009. A clathrin-dependent pathway leads to KRas signaling on late endosomes en route to lysosomes. *J. Cell Biol.* 184:863–879. http://dx.doi.org/10.1083/jcb.200807186

Niwa, H., K. Yamamura, and J. Miyazaki. 1991. Efficient selection for high-expression transfectants with a novel eukaryotic vector. *Gene.* 108:193–199. http://dx.doi.org/10.1016/0378-1119(91)90434-D

Ogura, E., Y. Okuda, H. Kondoh, and Y. Kamachi. 2009. Adaptation of GAL4 activators for GAL4 enhancer trapping in zebrafish. *Dev. Dyn.* 238:641–655. http://dx.doi.org/10.1002/dvdy.21863

Prior, I.A., C. Muncke, R.G. Parton, and J.F. Hancock. 2003. Direct visualization of Ras proteins in spatially distinct cell surface microdomains. *J. Cell Biol.* 160:165–170. http://dx.doi.org/10.1083/jcb.200209091

Ran, F.A., P.D. Hsu, J. Wright, V. Agarwala, D.A. Scott, and F. Zhang. 2013. Genome engineering using the CRISPR-Cas9 system. *Nat. Protoc.* 8:2281–2308. http://dx.doi.org/10.1038/nprot.2013.143

Rasmussen, S.G., B.T. DeVree, Y. Zou, A.C. Kruse, K.Y. Chung, T.S. Kobilka, F.S. Thian, P.S. Chae, E. Pardon, D. Calinski, et al. 2011. Crystal structure of the β2 adrenergic receptor-Gs protein complex. *Nature.* 477:549–555. http://dx.doi.org/10.1038/nature10361

Schmick, M., N. Vartak, B. Papke, M. Kovacevic, D.C. Truxius, L. Rossmannek, and P.I. Bastiaens. 2014. KRas localizes to the plasma membrane by spatial cycles of solubilization, trapping and vesicular transport. *Cell.* 157:459–471. http://dx.doi.org/10.1016/j.cell.2014.02.051

Schmidt, W.K., A. Tam, K. Fujimura-Kamada, and S. Michaelis. 1998. Endoplasmic reticulum membrane localization of Rce1p and Ste24p, yeast proteases involved in carboxyl-terminal CAAX protein processing and amino-terminal a-factor cleavage. *Proc. Natl. Acad. Sci. USA.* 95:11175–11180. http://dx.doi.org/10.1073/pnas.95.19.11175

Shao, D.D., W. Xue, E.B. Krall, A. Bhutkar, F. Piccioni, X. Wang, A.C. Schinzel, S. Sood, J. Rosenbluh, J.W. Kim, et al. 2014. KRAS and YAP1 converge to regulate EMT and tumor survival. *Cell.* 158:171–184. http://dx.doi.org/10.1016/j.cell.2014.06.004

Silvius, J.R., P. Bhagatji, R. Leventis, and D. Terrone. 2006. K-ras4B and prenylated proteins lacking "second signals" associate dynamically with cellular membranes. *Mol. Biol. Cell.* 17:192–202. http://dx.doi.org/10.1091/mbc.E05-05-0408

Tsai, F.D., M.S. Lopes, M. Zhou, H. Court, O. Ponce, J.J. Fiordalisi, J.J. Gierut, A.D. Cox, K.M. Haigis, and M.R. Philips. 2015. K-Ras4A splice variant is widely expressed in cancer and uses a hybrid membrane-targeting motif. *Proc. Natl. Acad. Sci. USA.* 112:779–784. http://dx.doi.org/10.1073/pnas.1412811112

Whyte, D.B., P. Kirschmeier, T.N. Hockenberry, I. Nunez-Oliva, L. James, J.J. Catino, W.R. Bishop, and J.K. Pai. 1997. K- and N-Ras are geranylgeranylated in cells treated with farnesyl protein transferase inhibitors. *J. Biol. Chem.* 272:14459–14464. http://dx.doi.org/10.1074/jbc.272.22.14459

Wright, L.P., and M.R. Philips. 2006. Lipid posttranslational modifications: CAAX modification and membrane targeting of Ras. *J. Lipid Res.* 47:883–891. http://dx.doi.org/10.1194/jlr.R600004-JLR200

Yona, S., H.H. Lin, W.O. Siu, S. Gordon, and M. Stacey. 2008. Adhesion-GPCRs: Emerging roles for novel receptors. *Trends Biochem. Sci.* 33:491–500. http://dx.doi.org/10.1016/j.tibs.2008.07.005